Isogeometric models for impact analysis with LS-DYNA

Mattia Montanari[1], Liping Li[2], Nik Petrinic[1]

[1] Department of Engineering Science, University of Oxford Parks, Road, Oxford, OX1 3PJ, UK
[2] Livermore Software Technology Corporation (LSTC), Las Positas Road, Livermore, CA 94551, US

Abstract

The advent of isogeometric analysis (IGA) opened new horizons for reducing design and optimization costs. By employing the same mathematical formulation to describe CAD and simulation models, IGA integrates design and analysis into a new paradigm. Our work is part of a technology validation effort that aims to assess IGA for the analysis of impacts.

Case studies of (i) wave propagation, (ii) material model calibration and (iii) ballistic impact are being conducted to compare the finite element analysis (FEA) against IGA. These case studies underpin the analysis of turbine fan blades and their containment casing (Figure 1). The IGA element formulation results more expensive than traditional FEA; however, it captures travelling stress waves more accurately. This improves significantly our ability to predict the dynamic response of systems, for example, undergoing high strain-rate loadings. Unfortunately, the mathematical formulation which makes IGA more accurate, does not allow discontinuities in the displacement field. This prevents, for example, a projectile to penetrate a target plate. It is argued that the physical failure can be predicted by using material models combining strain-rate-sensitive failure criteria.

This work uses a plug-in for LS-DYNA to generate analysis-ready CAD models, and the LS-DYNA parallel computing capabilities for assessing the applicability of IGA in impact problems.

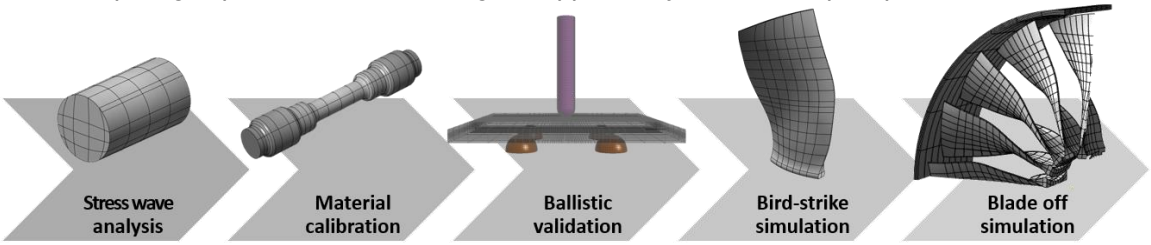

Fig.1: Isogeometric analysis-ready CAD models.

1 Introduction

Isogeometric analysis (IGA) was introduced with the primary goal of enabling Computer Aided Design (CAD) engineers and numerical analysts to work on the same geometry [1]. Indeed, IGA aims to circumvent one of the biggest limitation of the finite element analysis (FEA), that is, FEA can only approximate CAD geometries. This approximation limits the modelling fidelity, for example, in contact mechanics problems [7].

Moreover, IGA can reduce the costs of meshing and re-meshing with respect to FEA. In fact, IGA imports a coarse mesh from CAD into the analysis environment without changing the geometry. Afterwards, the mesh can be easily refined on-the-fly during the analysis.

There are however barriers to the applicability of IGA. Firstly, the behaviour of IGA solid elements is not well understood. Secondly, modern CAD models are collections of surfaces and thus not suitable for analysis of solid structures. It is mainly for these reasons that, to date, IGA has limited industrial applications.

This study aims to assess, and possibly expand, the applicability of IGA to mechanical problems involving complex geometries, failure and large models.

We develop a methodology for generating analysis-ready CAD models and use these for simulations of stress wave propagation and impact problems on solid structures. We use LS-DYNA because of its capability to run IGA simulations on Massively Parallel Processing (MPP).

Two test cases comparing IGA and FEA are presented: uni-axial pulse in cylindrical solid rod and ballistic test on titanium plate. The former provides insight on the accuracy of IGA for stress wave analysis, the latter tests the ability of IGA to predict failure and the ballistic limit of the target (i.e. the threshold velocity for which penetration occurs).

2 Method

2.1 NURBS-based isogeometric analysis

In order to have a unique geometry for both environments, CAD and analysis, a unique mathematical formulation describing the model must be chosen. Most modern CAD packages rely on non-uniform rational B-splines (NURBS) to discretize mechanical components. Therefore, a natural choice for IGA is to use NURBS in its isoparametric formulation.

A NURBS is a piecewise rational spline that can efficiently represent complex geometries and conics (e.g. circles and ellipses). The simplest NURBS object in R^n is the curve $\boldsymbol{C}(u)$ of order p defined as:

$$\boldsymbol{C}(u) = \frac{\sum_{i=0}^{m} w_i N_{i,p}(u) P_i}{\sum_{i=0}^{m} w_i N_{i,p}(u)} = \sum_{i=0}^{n} R_{i,p}(u) P_i \quad (1)$$

where P_i is a list of control points, each one associated to a weight w_i, and $N_{i,p}(u)$ are basis functions. The i-th spline is defined over a knot vector $\Xi = \{u_0, \dots, u_m\}$ which contains $m = n + p + 1$ knots in non-decreasing and non-uniform order. The first and last knots are repeated $p + 1$ times. The most common formulation of B-spline basis function for computer application is due to Cox and de Boor [3]. For further details on NURBS refer to [4, 5].

The tensor product construct is used to define NURBS surfaces and volumes. Examples of solid NURBS objects are illustrated in Figure 1. A (solid) volume body $\Omega \subset R^3$ is described by taking the tensor product of three NURBS, thus defining a trivariate function $\boldsymbol{P}(u_R, u_S, u_T)$ whose image is Ω – the three parametric dimensions are denoted with the following subscripts R, S, and T. A trivariate NURBS is therefore defined by:

$$\boldsymbol{P}(u_R, u_S, u_T) = \sum_{i=0}^{n_R} \sum_{j=0}^{n_S} \sum_{k=0}^{n_T} R_{i,p_R}(u_R) R_{j,p_S}(u_S) R_{k,p_T}(u_T) P_{i,j,k} \quad (2)$$

where all points $P_{i,j,k}$ form a three-dimensional grid of control points. To each weight $w_{i,j,k}$ is it associated one of these control points in order to generate the rational functions $R_{i,p_R}(u_R)$, $R_{j,p_S}(u_S)$ and $R_{k,p_T}(u_T)$ as in Eq. (1). It is important to notice that the solid NURBS in Eq. (2) is defined by three different polynomial orders (p_R, p_S, p_T), and three knot vectors ($\Xi_R . \Xi_S, \Xi_T$).

Similarly to finite elements, NURBS elements can be p- or h -refined (see [1] for k-refinement); however, higher-order NURBS shape function have an advantage over their finite element counterparts, that is, splines do not oscillate nor overshoot near discontinuities. While higher-order finite element polynomials yield to spurious numerical oscillation when interpolating a sharp discontinuity (so-called Gibbs phenomenon), NURBS do not [2]. Intuitively, a NURBS "cannot oscillate" more than its control grid and its higher-order formulation is therefore suitable for numerical analysis of non-smooth solutions.

2.1.1 Comparison between IGA and FEA

From the numerical analysis point of view, the most important difference between IGA and FEA is the definition and the formulation of the elements. While FEA have elements that can be grouped in subgroups to form a mesh, the IGA elements are defined by knots over a patch.

In practice IGA allows larger elements compared to FEA, and they can have different degree for each parametric direction; namely, Eq. (2) allows $p_R \neq p_S \neq p_T$. Further details may be found in [6], Table 1 summarizes some of the key differences.

Finite Element Analysis (FEA)	Isogeometric Analysis (IGA)
Mesh	Knots
Nodal points	Control points
Nodal variables	Control variables
Interpolant basis	Not Interpolant basis
Approximate CAD	Exact CAD
Polynomial basis	NURBS basis
Subdomains	Patches
Isoparametric paradigm	Isoparametric paradigm

Table 1: Brief comparison between FEA and IGA element formulations.

2.2 Generation of analysis-ready solid models

CAD models are assemblies of NURBS surfaces, these "hollow" models can only simulate thin structures. Moreover, the NURBS surfaces are often not watertight and this complicates the communication between CAD and analysis environments.

In order to assess IGA for large-scale and realistic models, we developed a plug-in for LS-DYNA that assists the generation of analysis-ready models from complex CAD geometries. For example, the tensile test specimen and the turbine fan blade illustrated in Figure 1 were generated from a CAD software.

The plug-in exports to LS-DYNA solid NURBS cards for IGA modelling. The model is a coarse, but exact, representation of the CAD geometry and is refined before the analysis. Figure 2 illustrates the functionality of the plug-in.

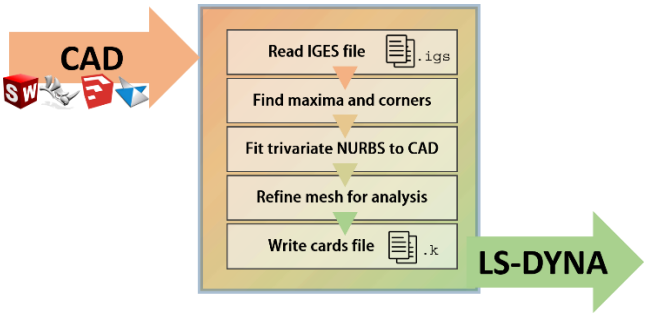

Fig.2: Workflow of LS-DYNA plug-in for generating IGA models from CAD.

2.3 Description of test cases

2.3.1 Stress wave in solid rod

A uni-axial compression test specimen is loaded axially and the propagating stress wave is analysed using IGA and FEA. This section describes the LS-DYNA model.

Specimen The geometry of the specimen is a cylindrical solid rod of diameter $d = 4.6\,mm$ and length $l = 8.0\,mm$. It is assumed elastic isotropic material, therefore **`*MAT_001`** is used, with Young's modulus $E = 1.04\,MPa$, Poisson ratio $\nu = 0.3$ and density $\rho = 8.0\,e-9 kg/m^3$.

Load A resultant force of $8010\,N$ is applied perpendicularly to one side of the rod, this is the *input face*. The load history is shown in Figure 3, where the *rising time* is $t_r = 1/10\,c$ and the *striker time* is $t_{st} = 9/10\,c$ for a speed wave $c = \sqrt{E/\rho}$.

Spatial discretization The solid rod is described using two discretisations: hexahedral finite elements **`*ELEMENT_SOLID`** and a single NURBS patch **`*ELEMENT_SOLID_NURBS_PATCH`**. The FEA model is obtained using the built-in meshing capability from LS-PrePost *cylinder solid* which requires, as inputs, the number of elements in circumferential and axial direction, respectively N_C and N_A. To generate the NURBS solid patch, the plug-in described in Section 2.2 is used. Two examples of FEA and IGA discretisation are illustrated in Figure 4.

Two levels of refinement are studied for both discretisation types. A coarse FEA mesh is built with $N_C = N_A = 80$, and a finer one with $N_C = N_A = 110$. The trivariate NURBS patches are defined by mapping the parametric direction T to the axial direction, and R, S to the cross section. A coarse patch is defined by 20 intervals between the extrema of knot vector $ Ξ_T and 6 intervals for Ξ_R, Ξ_S, and polynomial orders $p_T = 4$ and $p_R, p_S = 2$. This is then refined to obtain a finer patch by doubling the internals for each knot vector, and p-refining of two orders each parametric direction.

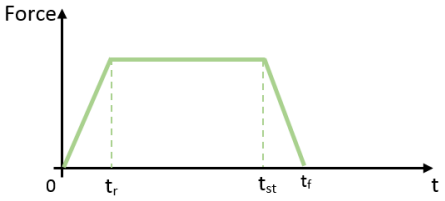

Fig.3: Axial pulse load history.

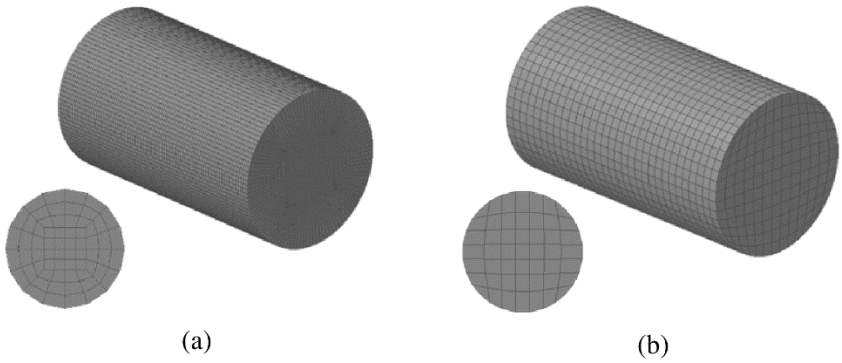

Fig.4: Spatial discretisation of solid rod with FEA (a) and IGA (b) – notice the different topology in the front view.

2.3.2 Ballistic test on Ti-6Al-4V plate

A numerical model of a ballistic test is simulated using LS-DYNA. The model includes a target, a projectile and four supports. For the sake of simplicity, friction is neglected and the supports are fixed. The test is repeated for two initial velocities of the projectile $225\ m/s$ (below the ballistic limit) and $275\ m/s$ (above the ballistic limit). This section describes the FEA and IGA models. All tests will be repeated using MPP to assess the scalability of each method.

Geometry The target is a squared $130\ mm$ x $130\ mm$ plate $7\ mm$ thick. The plate is mounted onto four fixed semi-spherical supports. The mass of the projectile is $67.3\ g$. The projectile has rounded nose and hits the target perpendicularly. Figure 5 illustrates the model.

Material models The titanium plate is modelled with an elasto-plastic material model with strain rate dependency **`*MAT_024`**. This was calibrated experimentally for three different strain rates: $\varepsilon_{low} = 1.\dot{0}e-3s^{-1}$, $\varepsilon_{med} = \dot{2}.52e2s^{-1}$ and $\varepsilon_{high} = \dot{2}.0e3s^{-1}$. The projectile is assumed linear elastic (**`*MAT_001`**) and the support rigid (**`*MAT_020`**).

Spatial discretisation For the discretisation of the target plate, solid brick finite elements and a trivariate NURBS patch are used. For both we use different levels of refinement. The FEA mesh needs to be particularly fine in order to reduce the hourglass effect, so we created a coarse and a finer mesh. Three IGA patches are generated: one relatively coarse, other two resulting from h- and p-refinement. The first two use quadratic shape functions in all parametric directions, the third patch uses fourth order through thickness.

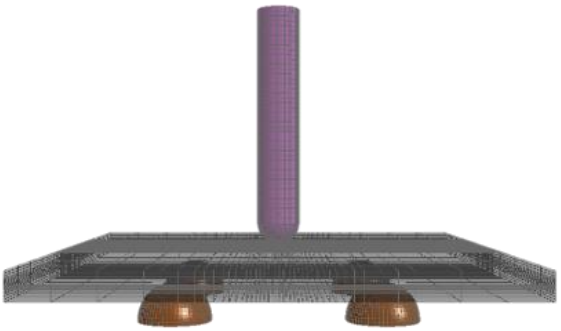

Fig.5: Perspective view of the ballistic test model.

3 Results

The numerical tests are carried out using LS-DYNA, the results on the CPU profiling times are generated from a Linux machine (Red Hat 5) running MPI 8.1.1 on Intel Xeon64®.

3.1 Stress wave in solid rod

For each one of the four FEA and IGA meshes, the tests are repeated using 1, 4 and 8 cores.
This section compares the performance and the Von Mises stress obtained with FEA and IGA.

Scalability The CPU time for each simulation is shown in Figure 6(a). As expected, the coarse FEA mesh runs faster, while the finer IGA mesh results doubles the CPU time due to the more expensive element formulation of the latter. However, by looking at the CPU time for the other two meshes, IGA seems to scale better than FEA. This is confirmed by the relative gain in Figure 6(b).
We can conclude that these (small) IGA models scale better on multiple cores than FEA. This is due to the more expensive element formulation of the former. Results are collected in Table 2.

Accuracy The Von Mises stress predicted by FEA and IGA are compared. Figure 7 shows the stress distribution when the front of the travelling stress wave first reaches the middle of rod. At the same time frame, Figures 8(a)-(b) show stress isosurfaces within the specimen. Figure 8(c)-(d) show isosurfaces when the front of the wave reaches the middle of the rod after bouncing back and travelling toward the input face.
Despite the IGA mesh topology (see Figure 4) introduces elements with poor aspect ratio, in all cases the stress distribution captured by IGA results significantly more homogeneous. This is a consequence of the higher-order formulation and the absence of Gibbs Phenomenon for NURBS [5].

Test ID	Method	p_R, p_S, p_T	Runtime 1 CPU	Runtime 4 CPUs	Runtime 8 CPUs
01	IGA	2, 2, 4	91 min	26 min	16 min
02	IGA	4, 4, 6	173 min	70 min	58 min
03	FEA	1	30 min	10 min	8 min
04	FEA	1	83 min	27 min	21 min

Table 2: Profiling results for the uni-axial pulse in solid rod test.

3.2 Ballistic test on Ti-6Al-4V plate

Test without penetration In all tests with low impact velocity, $v_i = 225\ m/s$,the projectile bounces back after hitting the target. Figure 10 shows the velocity (a) and the acceleration (b) of the projectile for the fine FEA mesh and three IGA mesh refinements. The velocities show good agreement until $t = 0.1\ s$. Good matching is also show for the final rebound velocity predicted by FEA and by the h-refined IGA model. Figure 10(a) also demonstrates that h-refinement has a higher impact on the final results than p-refinement. This fact is more evident in Figure 10(b), where the accelerations of the projectile are compared.
FEA predicts a stiffer response of the plate, leading to a higher maximum acceleration of the projectile.

Test with penetration Figure 11 compares the velocity of the projectile predicted by three IGA meshes and a fine FEA mesh. For the FEA simulations we use different hourglass controls methods. It should

be highlighted that for the ballistic test the effect of hourglass is particularly pronounced. All curves in Figure 11 match well until the plate breaks, afterwards all solutions diverge significantly. A direct comparison of projectile velocity and acceleration between FEA and IGA is shown in Figure 12.
Both methods predict failure. They initially return similar responses, until about $t = 0.05\ s$, afterwards the plate fails. Because of the simple material model employed for the target, we cannot compute the residual velocity of the projectile accurately. However, Figure 12(b) gives an estimate of when the target fails, and therefore what the ballistic limit of the plate is.
An important difference between for methods is the stress distribution within the plate. Figure 13 and Figure 14 illustrate at different time frames that, while FEA removes elements, IGA somehow increases the number of elements engaging with the projectile. This can be seen from larger area of elements with high values of stress.

Scalability The CPU profiling results from MPP simulations are reported in Figure 9(a) and Figure 9(b) for FEA and IGA, respectively. These figures show the CPU cost breakdown for each task of the simulations when using 32, 64 and 128 CPUs.
For both methods, the *element processing* task scales very well as the percentage of CPU time decreases as the number of CPUs increases. The *contact search algorithms* do not scale that well on multi-cores because contact information need to be exchanged between cores. In this model, the contact element are distributed to few cores only, other cores need to wait while these carry out the contact calculation. As a result, the waiting time increases significantly as the number of cores increases and is measured in the *time step size* task. An optimised decomposition may be applied to reduce the cost of this task. Similarly, *Misc. 3* accounts for costs due to memory management and communication between cores. This task also increases its cost with the number of cores.
From the relative cost of *time step size* and *Misc.3*, we can conclude that the ballistic test model using IGA is too small to benefit from the MPP capability of LS-DYNA. In fact, when using 64 or 128 CPUs, the overhead cost of communication between cores is comparable to the *element processing*. We did not anticipate this result, this suggests that IGA will not have problems to scale on “large enough” models.

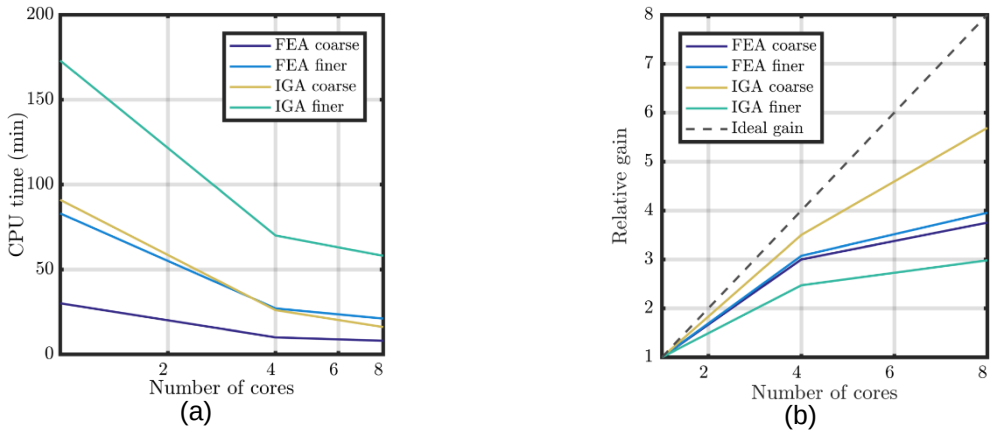

Fig.6: CPU time for solid rod test case. (a) Compares how CPU time of FEA and IGA scale for various levels of refinement as the number of cores increases. (b) Shows the relative gain for the same meshes.

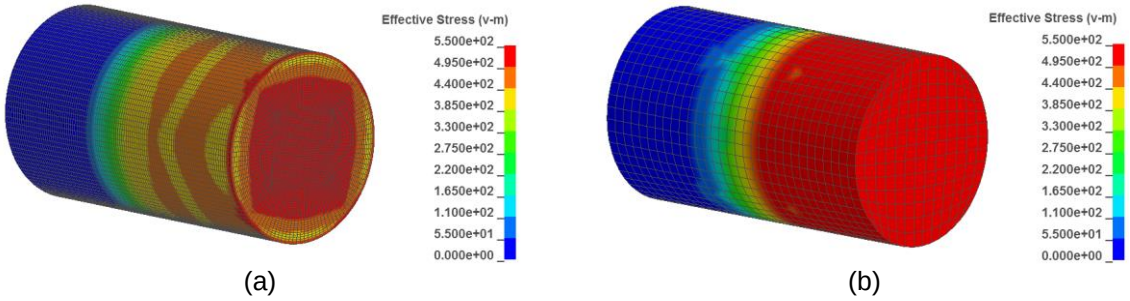

Fig.7: Compression of solid rod. Von Mises stress contour plot at $t = t_{st}/2$ for FEA (a) and IGA (b).

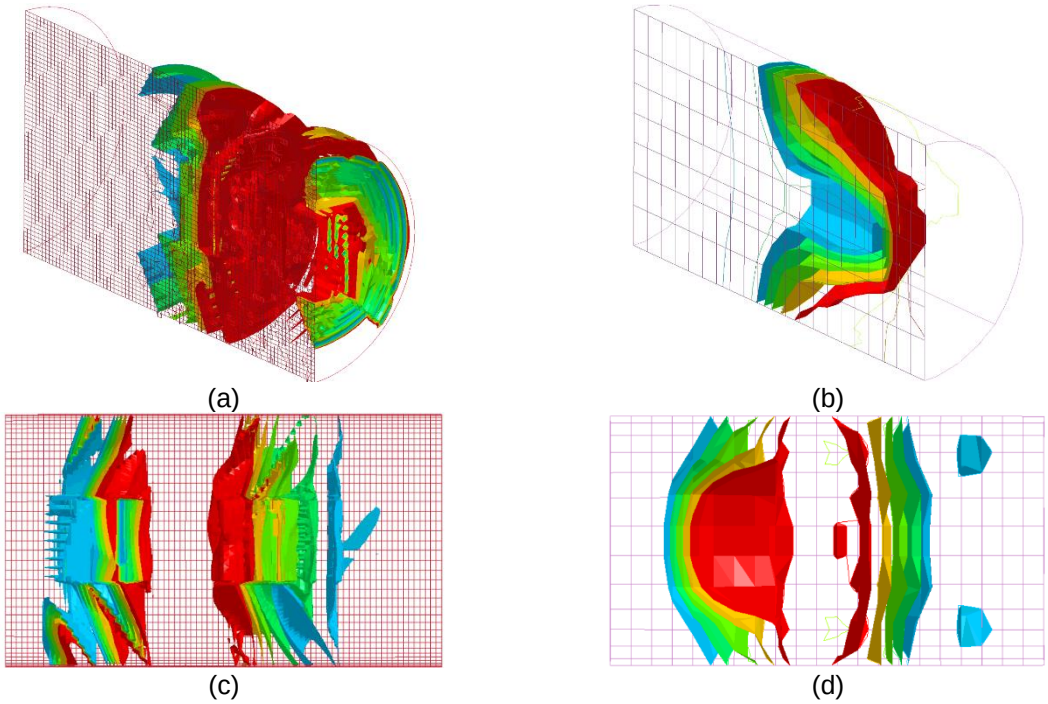

Fig.8: Von Mises stress distribution at $t = t_{st}/2$ for FEA (a) and IGA (b), and at $t = t_{st}/0.5$ for FEA (c) and IGA (d).

4 Conclusions

This work studied the applicability of isogeometric analysis (IGA) and the presented preliminary results were presented. Two test cases comparing FEA and IGA for the analysis of impacts were carried out.

Both methods seem to have comparable applicability, provided that solid IGA models can be imported directly from CAD. In order to provide LS-DYNA with analysis-read models, we built a plug-in which reads CAD models and creates solid NURBS geometries with identical geometry. Although with limited capabilities, we have shown that our methodology can import complex geometries (e.g. turbine fan blades).

From the analysis of the CPU time, IGA formulation is more expensive compared to standard finite elements; however, the Massively Parallel Processing (MPP) of LS-DYNA was not fully exploited in this work. In fact, the models presented in this work are sufficiently large to see the MPP benefits on FEA, but too small for IGA. Further studies may confirm that FEA and IGA scale equally well when solving larger models.

Acknowledgement

The authors gratefully acknowledge the financial support of this research by the UK Technology Strategy Board and Rolls-Royce plc through the Strategic Investment in LOw-carbon Engine Technology (SILOET 2) project.

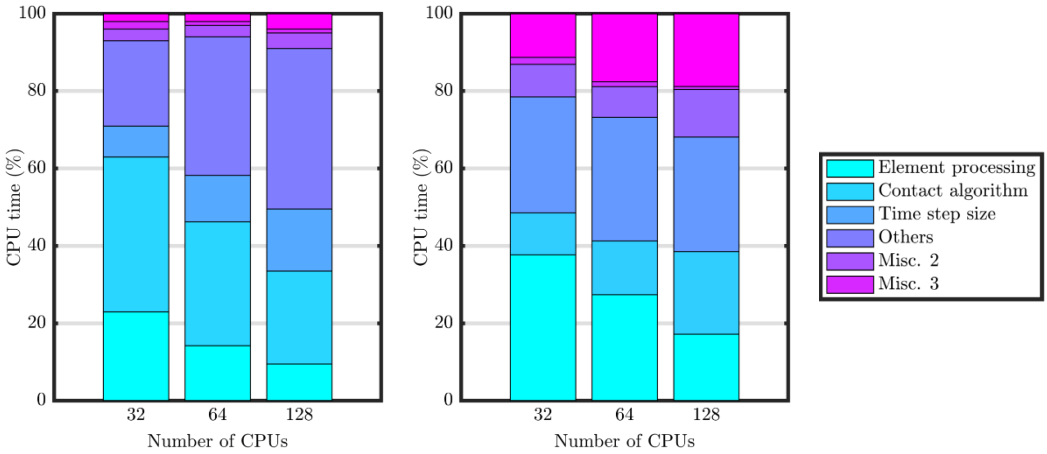

Fig.9: CPU profiling results for FEA (a) and IGA (b).

References

[1] Hughes, T. J. R. , Cottrell, J. A. , and Bazilevs, Y., (2005). Isogeometric analysis: CAD, finite elements, NURBS, exact geometry and mesh refinement Comput. Meth. Appl. Mech. Eng., 194:4135-4195.
[2] Trefethen, Lloyd N. (2013). Approximation theory and approximation practice, SIAM.
[3] De Boor, C. (1978). A Practical Guide to Splines. Springer-Verlag.
[4] Schoenberg, I. J., Greville, T. N. E., (1967). On spline functions. Inequalities, 1:255-291.
[5] Piegl L., Tiller, W., (1997). The NURBS Book. Springer.
[6] Cottrell, J. A., Hughes, T. J. R. , and Bazilevs, Y., (2009). Isogeometric Analysis: Toward Integration of CAD and FEA. John Wiley & Sons.
[7] De Lorenzis L., Wriggers P., and Hughes T. J. R., (2014) Isogeometric contact: a review, GAMM-Mitteilungen, 1:85:123.

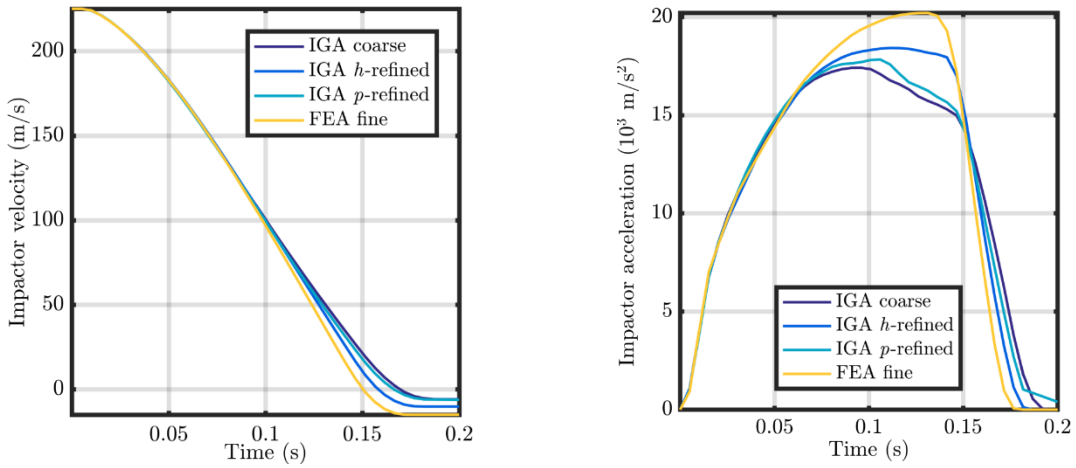

Fig.10: Non-penetrating ballistic test: comparison of FEA and IGA results for projectile velocity (a) and acceleration (b).

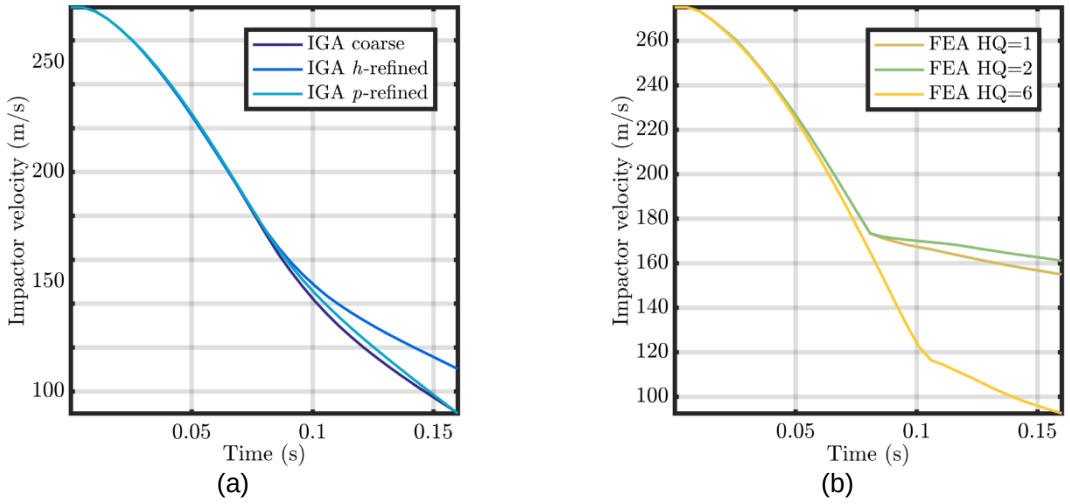

Fig.11: Projectile velocity for ballistic test with penetration: mesh sensitivity analysis for IGA (a), and comparison of different hourglass control (HQ) methods for FEA (b).

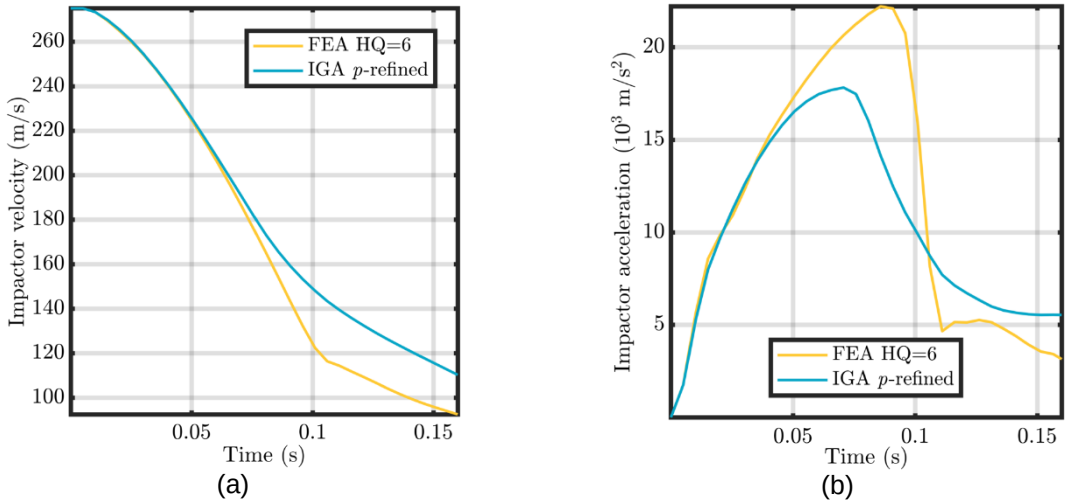

Fig.12: Comparison of projectile velocity (a) and acceleration (b) for penetrating ballistic test using FEA and IGA.

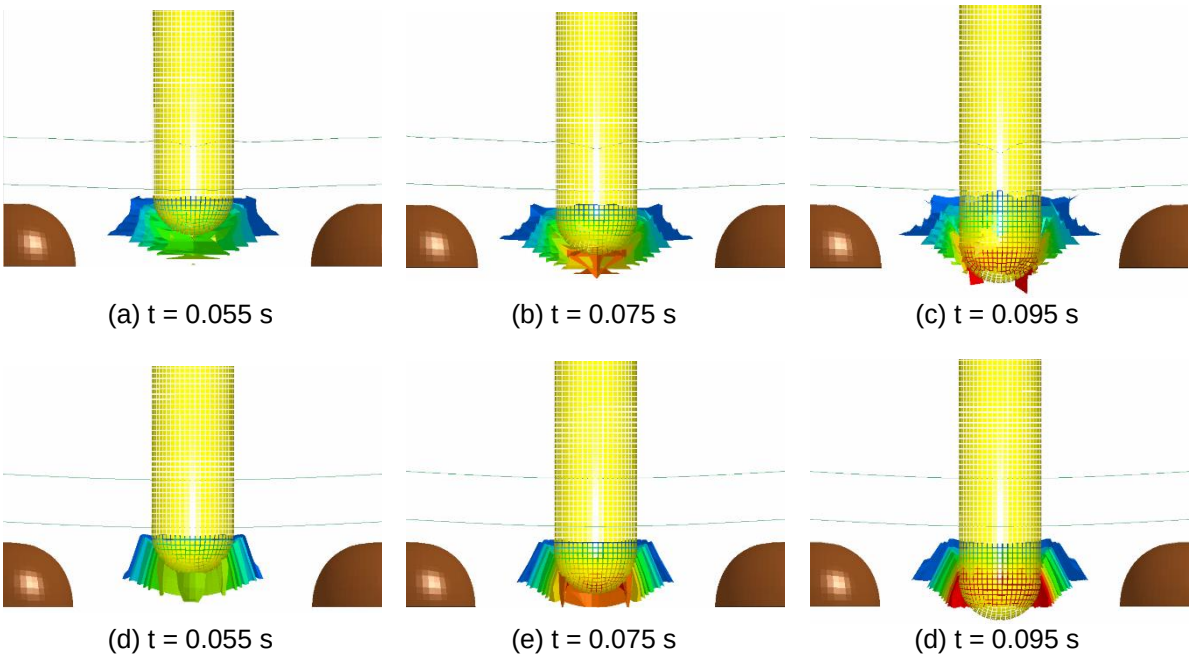

Fig.13: Section view of Ti-6Al-4V target plate with plastic strain isosurfaces of FEA (a)-(c) and IGA (d)-(f) at different time t.

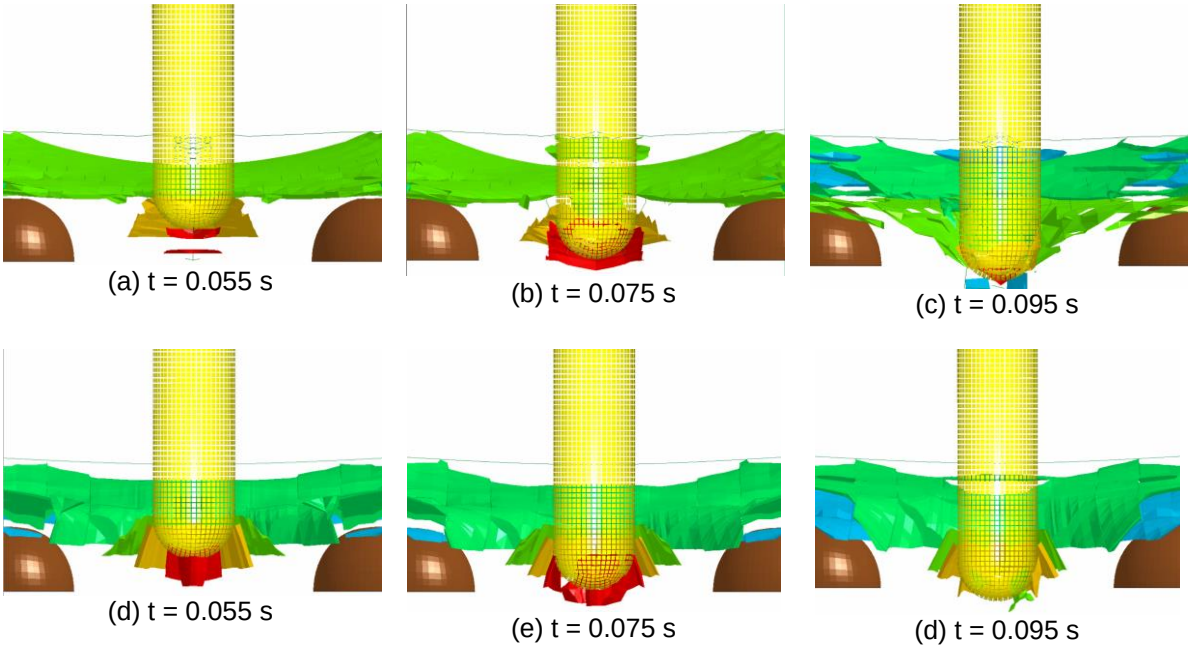

Fig.14: Section view of Ti-6Al-4V target plate with Von Mises stress isosurfaces for FEA (a)-(c) and IGA (d)-(f) at different time t.